IROS Workshop on Visual Control of Mobile Robots (ViCoMoR 2012)
October 11th, 2012, Vilamoura, Algarve, Portugal

Target Tracking and Obstacle Avoidance for a VTOL UAV using Optical Flow

Aurélie Treil[1], Philippe Mouyon[1], Tarek Hamel[2], Alain Piquereau[1] and Yoko Watanabe [1]

***Abstract*— This paper presents the practical implementation of a nonlinear visuel servo controller for obstacle avoidance and target tracking of an eye-in-hand Vertical Take-Off and Landing Uninhabited Air Vehicle (VTOL UAV). The VTOL vehicle is assumed to be equipped with a minimum sensor suite; a camera and Inertial Measurement Unit (IMU). The control law uses optical flow calculated from the camera images and angular measurement from IMU to ensure obstacle avoidance and target tracking of the UAV while maneuvering over a textured terrain made of planar surfaces. The proposed controller has been tested in simulation as a preliminary step to outdoor flight experiments. Both simulation and experimental results are presented in this paper.**

I. INTRODUCTION

Most of progresses in aeronautics field since the appearance of aircraft are due to military applications. UAVs are not an exception. They are born to limit losses of human pilot lifes during recognition missions. Operation fields, that require the use of UAV, are often urban environment. There are also some civil applications like monitoring traffic congestion, regular inspection of infrastructure such as bridges, etc. The urban environment brings new constraints to UAV operation. Indeed, masking of GPS signals by building walls in the city disables its use. Moreover to follow streets, which can be narrow, or even inside buildings UAVs need to be light and small. Finally, UAVs can be lost during mission, which implies cost constraint.

So, new solutions have been studied to compensate non-availability of GPS in urban environment and to go beyond cost and size constraints. In particular, visual servoing has been for twenty years an important research subject in ground robotics field and more recently in UAV field.

Visual servoing for ground applications has been extensively studied. Question of docking [1] and obstacle detection and avoidance [2], [3] have been treated. For example to detect obstacle, methods using perspective have been set up [4] as well as method based on optical flow [5]. In UAV category optical flow is often used in biomimetic approaches [6], [7], [8]. Optical flow is also used combined with IMU measurements for stabilisation and vertical landing problematics, [9], [10] and for terrain following applications, [11].

Two objectives are identified in this paper. The first is the target tracking for a VTOL UAV, the second is the obstacle avoidance during tracking, by using vision and IMU. Image features considered are the optical flow obtained from image processing algorithms, and using additional information provided by an embedded IMU for derotation of the flow. A non-linear proportional type controller is designed for target tracking. This controller is augmented with a repulsive action via repulsive potential fields around obstacles.

To expose this work we start, in Section II, by presenting the fundamental equations of motion for a VTOL UAV and describing the translational optical flow that is used as an input for the control law. Section III presents the control strategy for target tracking and obstacle avoidance manoeuvres. Section IV describes gain tuning and test in simulation. Section V is about image processing algorithms evaluation. Then, experimental results are presented in Section VI. Finally we conclude and discuss about futur work in section VII.

II. MODELLING

A. UAV dynamics model for control law design

The VTOL UAV is represented by a rigid body of mass m and of tensor of inertia J. To describe the motion of the UAV, two reference frames are introduced: an inertial frame $\mathcal{F}_I$ fixed on the ground and associated with the vector basis $[e_x, e_y, e_z]$ and a body-fixed frame $\mathcal{F}_B$ attached to the UAV at the center of mass and associated with the vector basis $[e_x^b, e_y^b, e_z^b]$.
A translational force F and a torque Γ are applied to the UAV. The translational force F combines thrust, lift and drag. The gravitational force can be separated from F. For a miniature VTOL UAV in quasi-stationary flight, one can reasonably assume that the aerodynamic forces are always in direction e_z^b, since the lift predominates on the other components. Let ξ, v, be the UAV position and velocity in $\mathcal{F}_I$, R the rotation matrix from $\mathcal{F}_B$ to $\mathcal{F}_I$ and Ω the angular velocity in $\mathcal{F}_B$. Then, the UAV dynamics can be written as:

$$\begin{cases} \dot{\xi} = v \\ m\dot{v} = F + mge_z, \quad F = RTe_z^b \\ \dot{R} = R\,\mathrm{sk}(\Omega) \\ J\dot{\Omega} = -\Omega \times J\Omega + \Gamma \end{cases} \tag{1}$$

with T the rotor thrust and g the gravity. sk(.) denotes the skew-symetric matrix representing cross-product.

The VTOL UAV is equipped with a minimum sensor suite, IMU which provides Ω and R, and a camera. For the rotational dynamics of the UAV, a high gain controller is used to ensure that the orientation R of the UAV converges

[1]ONERA, Dept. of Systems Control and Flight Dynamics, Toulouse, France, firstname.name at onera.fr
[2]I3S, CNRS, Sophia Antipolis, France, thamel at i3s.unice.fr

to the desired values. The resulting control problem is then simplified to:

$$\dot{\xi} = v, \quad m\dot{v} = F + mge_z \tag{2}$$

Thus in the part III, only the control of the translational dynamics (2) is considered and the direct control input, $u = F$. This common approach is used in practice and can be justified theoretically using singular perturbation theory [12].

B. Translational optical flow for visual servoing

The translational optical flow on a spherical image, under the following assumptions is presented in the sequel.

Assumption 1:

- The camera is positioned at the UAV center of mass, with its orientation aligned with $\mathcal{F}_B$ and the optical axis is e_z^b,
- Points of the environment are stationary in the inertial frame. Thus, motion of the environment points appeared on images depends only on motion of the camera,
- Surface observed is textured and plane.

The choice of using spherical image is based on the passivity-like property discussed in [13] and the fact that it is possible to convert optical flow and points position in a plane image to a spherical image [14].

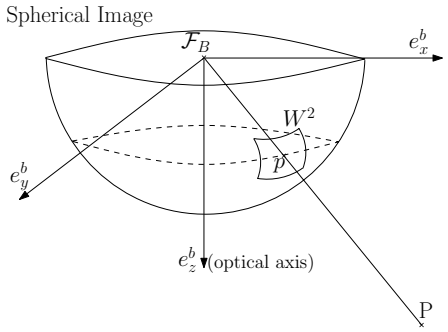

Fig. 1. Spherical Image

Let $P = (X, Y, Z)^T$ be the position of a point on the surface observed expressed in $\mathcal{F}_B$. Figure 1 shows its projection on a unit radius spherical image $f = 1$. The projection equation is given by:

$$p = \frac{P}{|P|} \tag{3}$$

where $|.|$ denotes the Euclidean norm.

Introducing the normal direction η, expressed in $\mathcal{F}_B$, to the surface, the distance to its surface can be written:

$$d =< P, \eta >= |P| < p, \eta > \tag{4}$$

where <.,.> is the inner product. As defined in [15], the translational optical flow is:

$$w = -\frac{v}{d} = RQ^{-1}(\dot{q} + \Omega \times q) \tag{5}$$

where,

$$q = \sum_{i=1}^{n} p_i \tag{6}$$

with p_i the set of points on W^2 (Fig.1), a section of the image. The square matrix Q is defined by :

$$\begin{aligned} \dot{q} &= \sum_{i=1}^{n} \dot{p}_i \\ &= -\Omega \times q - \sum_{i=1}^{n} \left(I - p_i p_i^T\right) < p_i, \eta > R^T \frac{v}{d} \\ &= -\Omega \times q - QR^T \frac{v}{d} \end{aligned} \tag{7}$$

III. TARGET TRACKING AND OBSTACLE AVOIDANCE

A. Target tracking

In this section a control design for target tracking is proposed. Let call target a point of the environment that the UAV has to join. This control law is inspired by [9]. The translational optical flow and the target position on the image are used as an input. The target is a point on the horizontal and plane ground ($R\eta = e_z$). Its coordinates expressed in $\mathcal{F}_I$ are ${}^I P$. The target error expressed in $\mathcal{F}_B$ is thus

$$P = R^T({}^I P - \xi) \tag{8}$$

Its projection on the spherical image is denoted p ans is merged with the target location within the image.

Proposition 3.1: Consider the dynamics (2) and assume that the thrust vector $u = F$ is the control input chosen as follows:

$$u = -mge_z + mk_P(w + k_I Rp), \ k_P, \ k_I > 0 \tag{9}$$

The proof that $\forall t$, $d(t) > 0$ and hence the linear velocity and the position of the UAV converges asymptotically towards zero, is done by using a Lyapunov function. The proof is not presented here but will be the object of a future article.

B. Obstacle avoidance

In this section an obstacle avoidance control design is proposed augmenting the previous target tracking control law. The control law is inspired by [3] and the potential field theory.

1) Avoiding a unique obstacle: First, consider only one obstacle. Let P_o be a point on the obstacle surface, its position on the spherical image is named p_o and B_o be the spherical influence area around the obstacle, in which it is repellant, see Figure 2.

Assumption 2: The target position and the UAV initial position are not inside B_o.

Assumption 3: Obstacle is spherical and its volume is small, so the approximation $p_o = \eta_o$ can be made, with η_o the normal direction to the obstacle. To compute the translational optical flow of the obstacle, the surface around P_o is considered locally plane.

The distance to the obstacle can be writen as follows :

$$d_o =< P_o, \eta_o >= |P_o| \tag{10}$$

As defined in (5) the translational optical flow of the obstacle, w_o, is :

$$w_o = -\frac{v}{d_o} \tag{11}$$

The relative speed to the obstacle in the normal direction can be written as:

$$\begin{aligned}\frac{\dot{d}_o}{d_o} &= \frac{1}{d_o}\left(\eta_o^T \dot{P}_o + \dot{\eta}_o^T P_o\right) \\ &= \eta_o^T R^T w_o\end{aligned} \tag{12}$$

Since $\eta_o = p_o$, the control law hereafter uses an integration of $p_o^T R^T w_o$ to compute $\ln(d_o/d_o(0))$ up to a constant.

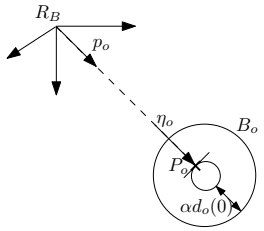

Fig. 2. Obstacle configuration

Proposition 3.2: Consider the dynamics (2) and assume that the thrust vector $u = F$ is the control input chosen as follows:

$$\begin{cases}\dot{\gamma} = p_o^T R^T w_o, \quad \gamma(0) = -\ln(\alpha) \\ u = -mge_z + mk_P(w + k_I Rp) + mk_o f(\gamma) Rp_o\end{cases} \tag{13}$$

with, $0 < \alpha < 1$, $k_P,\ k_I,\ k_o > 0$, and $f(\gamma) = \min(\gamma, 0)$.

Then, the UAV is ensured to avoid the obstacle, to get out of B_o, the repulsive sphere of radius $\alpha d_o(0)$ in a finite time if it enters in, to do never go back in B_o, and to converge asymptotically to the target if

$$k_o > \frac{k_I k_P |P(0)| + v(0)^T v(0)}{\alpha d_o(0)} \tag{14}$$

This constraint depending on the initial distance to the obstacle, UAV initial condition, and control gain of target tracking, determines how important has to be the repulsion. The proof is not presented here but will be the object of a future article.

2) Avoiding more than one obstacle: Considering more than one obstacle and calling B_{o_i} the influence sphere around the ith obstacle.

Assumption 4: B_{o_i} doesn't intersect an other influence sphere B_{o_j}, $\forall i \neq j$, otherwise they are merged in a unique repulsive sphere. B_{o_i} doesn't contain the target, $\forall i$.
As in previous section, the distance to the i^{th} obstacle can be written as follow :

$$d_{o_i} = |P_{o_i}| < p_{o_i}, \eta_{o_i} > \tag{15}$$

Using (5), the translational optical flow of the i^{th} obstacle, w_{o_i} is

$$w_{o_i} = -\frac{v}{d_{o_i}} \tag{16}$$

and the relative speed normal to the i^{th} obstacle,

$$\frac{\dot{d}_{o_i}}{d_{o_i}} = \eta_{o_i}^T R^T w_{o_i} \tag{17}$$

Proposition 3.3: Consider the dynamics (2) and assume that the thrust vector u is the control input chosen as follows

$$\begin{cases}\dot{\gamma}_i = p_{o_i}^T R^T w_{o_i}, \quad \gamma_i(0) = -\ln(\alpha_i) \\ u = -mge_z + mk_P(w + k_I Rp) + mk_{o_i} \sum_{i=1}^{n} f(\gamma_i) Rp_{o_i}\end{cases} \tag{18}$$

with, $0 < \alpha_i < 1$ and $k_P,\ k_I,\ k_{o_i} > 0$.

Then, the UAV is ensured to avoid each obstacle, to get out of each B_{o_i} in a finite time if it enters in, to do never go back in, and to converge asymptotically to the target if

$$k_{o_i} > \frac{k_I k_P |P(0)| + v(0)^T v(0)}{\alpha d_{o_i}(0)} \tag{19}$$

The proof is not presented here but will be the object of a future article.

IV. TEST IN SIMULATION

Control laws presented in part III are tested in simulation. First, the control gain are determined by considering the translational controlled dynamics for target tracking :

$$d\ddot{\xi} + k_P \dot{\xi} + k_P k_I' \xi = 0 \tag{20}$$

where $k_I' = k_I < p, \eta >$. Choosing a double pole at -0.5 and that for d^*=5m the damping ratio be 0.7. Solving the following equations,

$$\begin{cases} k_P^2 - 4dk_P k_I' = 0 \\ \dfrac{-k_P}{2d} = -0.5 \\ \dfrac{\sqrt{-k_P^2 + 4d^* k_P k_I'}}{-k_P} = -1 \end{cases} \tag{21}$$

it comes k_P=2.5 and k_I'=0.25.

Figure 3 shows the architecture of the simulator that includes in the complete UAV dynamics (1).

Control input are T, ϕ_c, θ_c and can be expressed as following:

$$\begin{aligned} T &= |u| \\ \phi_c &= \text{atan}\left(\frac{u_y}{|u_z|}\right) \\ \theta_c &= -\text{atan}\left(\frac{u_x}{|u_z|}\right) \\ \psi_c &= 0 \end{aligned} \tag{22}$$

The attitude controller on the ONERA UAV is :

$$\Gamma = k_1 \left(\begin{pmatrix} \phi_c - \phi \\ \theta_c - \theta \\ \psi_c - \psi \end{pmatrix} - k_2 \Omega \right) \tag{23}$$

with $k_1 = 3$ and $k_2 = 960$.

Figure 4 presents simulation results of UAV position and velocity for the target tracking with the initial conditions : $\xi(0) = [20; 20; -20]$, $v(0) = [0; 0; 0]$. The skid height is taken into account so simulation stops when the center of mass reach the height of 20 cm. Note that for the target tracking orientation dynamics introduce a difference between trajectory and velocity in (x, y) and in z. The maximum

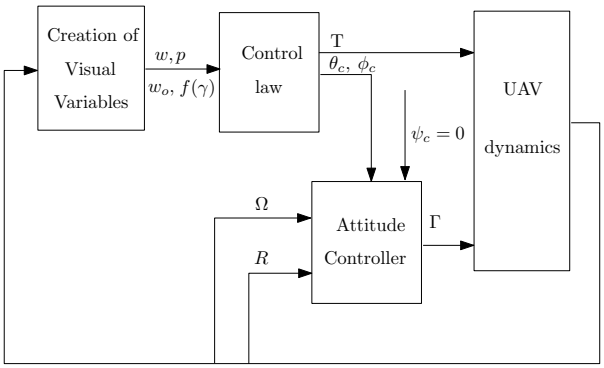

Fig. 3. UAV complete dynamics simulator

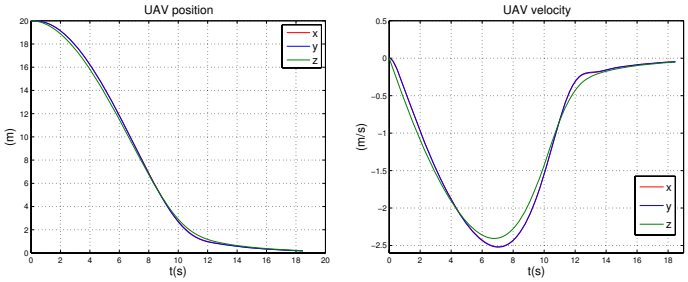

Fig. 4. UAV position and velocity

impact velocity of the UAV on the ground has to be 0.5m/s, this constraint is respected, see Figure 4 and 5.

Figure 5 is that for the obstacle avoidance with $k_o = 21$ and $\alpha = 0.5/d_o(0)$. Initial conditions are the same that for target traking, and the obstacle position in $\mathcal{F}_I$ is $P_o = [3; 3; -2.5]$. UAV 3D trajectory is shown in figure 6. The UAV reaction during the obstacle avoidance is slow due to the delay introduced by the orientation dynamics.

Figure 7 is the simulation results of target tracking with measurement noise on optical flow. The white noise introduced is based on noise estimation presented in the next part. Even with the noise the target tracking and obstacle avoidance is correctly realised.

Moreover, in the simulator the simulation stops when the target get out of the camera field of view. Because the control imposes a 3D deplacement with a constant slope and considering initial condition $v(0) = 0$, it is possible to determine the domain of acceptable UAV initial positions

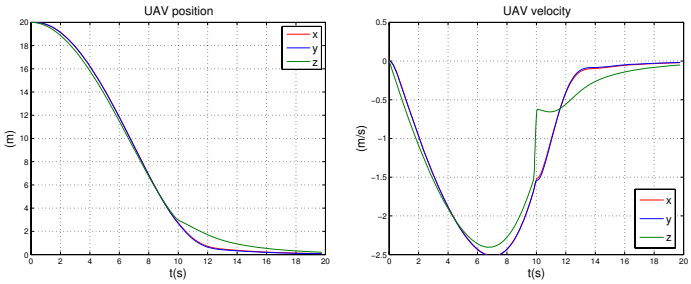

Fig. 5. UAV position and velocity in obstacle avoidance scenario

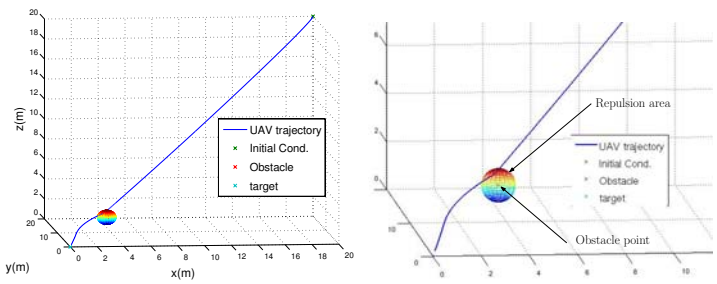

Fig. 6. UAV 3D trajectory with aobstacle avoidance and zoom on the repulsive area

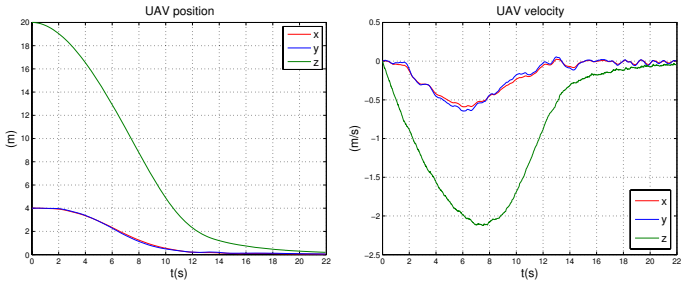

Fig. 7. Target tracking with noisy w,$v(0) = 0$, $\xi(0) = [4; 4; -20]$

for which the target stays in the camera field of view, see Figure 8.

V. IMAGE PROCESSING

This part presents the study of the image processing algorithms and their ouput. The precision of the measurements and the impact of the hypothesis previously made are studied. Image processing algorithms are runned on images of the onboard camera, recorded during flight test. The camera embedded on the ONERA VTOL UAV is a plane camera.

In the sequel are considered only image processing functions that yield to algorithms estimating affine deplacement between images. Calling p the coordinates of a point in the previous image, p' in the currant image, $A|b$ the affine deplacement matrix and H the homographic matrix. The affine deplacement can be written

$$p' = \begin{pmatrix} A & b \\ 0 & 1 \end{pmatrix} p = Hp \tag{24}$$

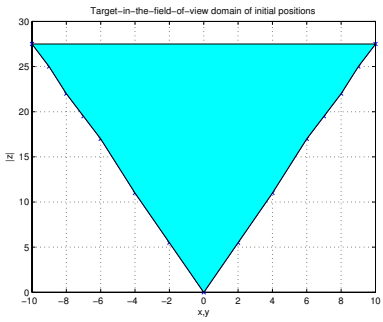

Fig. 8. Initial position from where target stays in the field of view

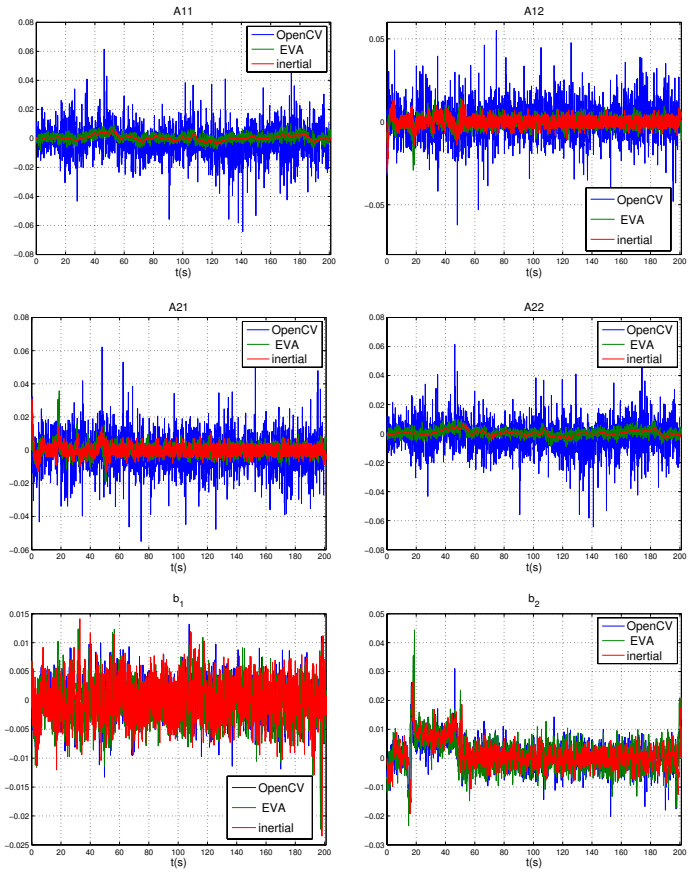

Fig. 9. $A|b$ and $A^*|b^*$

There exists a difference between real affine deplacement $A|b$ and its estimation named $A^*|b^*$. The relation between $A|b$ and $A^*|b^*$ is modeled as

$$\begin{aligned} A^* &= A + \bar{e}_A + \sigma_A \nu \\ b^* &= b + \bar{e}_b + \sigma_b \nu \end{aligned} \tag{25}$$

where, ν is a white noise, $\bar{e}_{A,b}$ and $\sigma_{A,b}$ are respectively the mean of error and the standard deviation of error on A or b.

Two image processing algorithms are compared to determine the most adapted to obtain $A^*|b^*$. The first uses OpenCV, an open source library of image processing functions. The second uses EVA a library equivalent to OpenCV developped by the ONERA/DTIM department. Both algorithms, the one based on OpenCv functions and the one based on EVA functions, provide affine deplacement between consecutive images. Steps that conduce to affine deplacement estimation are: feature point extraction from the previous and current image, matching of the two sets of points based on descriptor, estimation of the affine deplacement.

Figure 9 presents the value of $A|b$ obtained from GPS measurement, considered as true, and their estimations $A^*|b^*$ obtained with the image processing algorithm based on OpenCV functions and with the image processing algorithm based on EVA functions. These datas have been obtained from flight experimental measurements recorded during a representative trajectory of target tracking.

Algorithm	Term of Alb	Mean of error	Standard deviation
EVA	A_{xx}	-1.1543e-04	0.0022
	A_{xy}	1.4080e-04	0.0032
	A_{yx}	-2.0342e-04	0.0034
	A_{yy}	3.6142e-04	0.0038
	b_x	-0.0391	2.0141
	b_y	0.9360	2.9976
OpenCV : Harris + EstimateRigidTransform	A_{xx}	0.0025	0.0110
	A_{xy}	-7.8512e-04	0.0114
	A_{yx}	9.7957e-04	0.0120
	A_{yy}	-5.3694e-04	0.0116
	b_x	-0.0413	2.0106
	b_y	0.9741	3.0523

TABLE I
MEAN OF ERROR AND STANDARD DEVIATION

Table I shows mean and standard deviation of error of each componant of A and b. $\bar{e}_{A,b}$ and $\sigma_{A,b}$ have been calculated from datas presented on the Figure 9, in the case of OpenCV based image processing algorithm and on EVA based image processing algorithm. During this test it has been noticed that the calculation time for the entire operation chain on a 200x200 section of image is about 60ms for EVA and 20ms for OpenCV.

For flight experiment in section IV image processing algorithm based on EVA will be used because it is the more accurate of the two algorithms.

Moreover, it is possible to link $A|b$ to w writing theoretically the affine deplacement. Let Z be the distance to the ground along the optical axis and $V = (V_x, V_y, V_z)^T$ and ${}^b\Omega$ be the velocity and the angular velocity in $\mathcal{F}_B$ and considering that the center of the image section, on which the image processing algorithm is used, coincides with the center of the entire image, it comes (24) with

$$A = I + \begin{pmatrix} \frac{V_z}{Z} & -\Omega_z \\ \Omega_z & \frac{V_z}{Z} \end{pmatrix} dt \tag{26}$$

and

$$b = f \begin{pmatrix} \Omega_y - \frac{V_x}{Z} \\ -\Omega_x - \frac{V_y}{Z} \end{pmatrix} dt \tag{27}$$

Remark that because $\Omega = (\Omega_x, \Omega_y, \Omega_z)^T$ is measured, it is possible to isolate from $A|b$ the term $\frac{V}{Z}$. Using previous assumption of plane and horizontal ground it is possible to link $\frac{V}{Z}$ to w. In reality $A^*|b^*$ are estimated so it is possible to estimate w^*, that will be used in the control laws.

$$w^* = R \begin{pmatrix} \frac{1}{f.dt} b^* - \begin{pmatrix} \Omega_y \\ -\Omega_x \end{pmatrix} \\ \frac{1 - A^*_{11}}{dt} \end{pmatrix} \tag{28}$$

where A^*_{11} is the first row and first column coefficient of the A^* matrix. Because $A^*|b^*$ is noisy w^* is too. A discrete low pass filter is used to filter w^* .

VI. EXPERIMENTAL RESULTS

In order to realise the final scenario of target tracking and obstacle avoidance a plan of experiments is built. First, the work consists in testing control laws in the horizontal plane, the vertical control is managed by a control law using GPS

Fig. 10. ONERA RMAX UAV

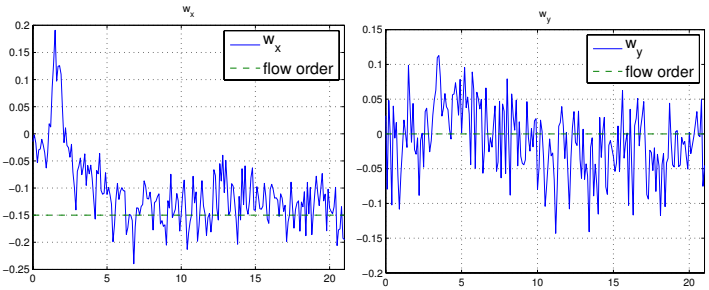

Fig. 11. Experimentation result of constant optical flow in x

datas. Then, the scenario is to move on the x axis with a constant optical flow. Second step is to run the horizontal target tracking. After that the vertical landing is tested to finally run the entire scenario of target tracking in 3D. Then, the same steps are realised with obstacle avoidance. The first step of this plan of experiments is presented in this part. For a move on the x axis with a constant optical flow the control law (9) is reduced to u_x and u_y the two first componants of the control u :

$$\begin{aligned} u_x &= mk_P(w_x + \alpha) \\ u_y &= mk_P(w_y + k_I \int w_y) \end{aligned} \tag{29}$$

where w_x, w_y are the two first componants of w and $\alpha = 0.15$ is the constant optical flow order in x. Initial conditions of the experiment are $v(0) = 0$, $\xi(0) = (0, 0, -20)$. The experiments are realized with an YAMAHA RMAX, Figure 10, on which are embedded the IMU, the camera and a PIP22 allowing the image processing and the control to be embedded. Figure 11 shows that the optical flow in x reaches its reference value. Because the UAV is at the same height during the flight and the ground is horizontal the UAV velocity reaches a constant value, see Figure 12. This experimentation shows that it is possible to control VTOL UAV in real time using optical flow, with an embedded camera and image processing system. Other parts of the plan of experiments are in progress so they are not presented here.

VII. Conclusion

This paper presented a nonlinear controller for obstacle avoidance and target tracking of a VTOL UAV using the measurement of optical flow along with the IMU data. The proposed control algorithm has been tested in simulation in different scenarios to demonstrate the performance of the closed loop system. And a first experimental result shown

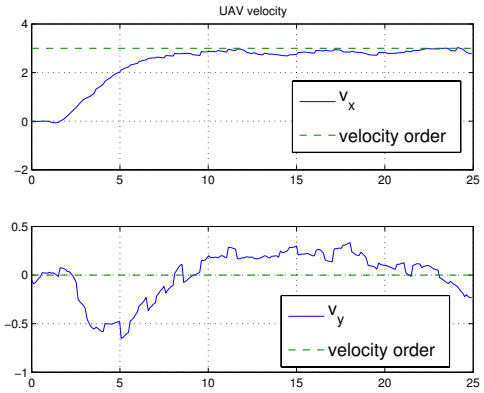

Fig. 12. UAV velocity during first experiment

that it was possible to achieve a closed-loop flight. As a futur work, we would like to complete experimental results with the entire scenario of target tracking and obstacle avoidance.

References

[1] J. Santos-Victor and G. Sandini, "Visual behaviors for docking," *Computer Vision and image understanding*, vol. vol 67, pp. pp 223–238, September 1997.

[2] J. Vanualailai, B. Sharma, and S. ichi Nakagiri, "An asymptotically stable collision-avoidance system," *International Journal of Non-Linear Mechanics*, vol. 43, pp. 925–932, 2008.

[3] E. P. Jiangmin Chunyu, Zhihua Qu and M. Falash, "A new reactive target-tracking control with obstacle avoidance in a dynamic environment," in *American Control Conference*, 2009.

[4] N. Simond, "Obstacle Detection from IPM and Super-Homography," in *IEEE IROS 2007 / International Conference on Intelligent Robots and Systems*, (San Diego, California / USA United States), IEEE Intelligent Robots and Systems, 10 2007.

[5] J. Santos-Victor and G. Sandini, "Visual-based obstacle detection. a purposive approach using the normal flow," *Intelligent Autonomous Systems*, 1995.

[6] J. S. Humbert and A. M. Hyslop, "Bioinspired visuomotor convergence," *Trans. Rob.*, vol. 26, no. 1, pp. 121–130, 2010.

[7] J.-C. Zufferey, *BIO-INSPIRED VISION-BASED FLYING ROBOTS*. PhD thesis, EPFL, 2005.

[8] F. Ruffier and N. Franceschini, "Octave, a bioinspired visuo-motor control system for the guidance of micro-air vehicles," in *Conference on Bioengineered and Bioinspired Systems*, 2003.

[9] B. Herisse, F.-X. Russotto, T. Hamel, and R. Mahony, "Hovering flight and vertical landing control of a vtol unmanned aerial vehicule using optical flow," in *IEEE/RSJ Internationnal Conference on Intelligent Robots and Systems*, 2008.

[10] B. Herisse, T. Hamel, R. Mahony, and F.-X. Russotto, "Landing a VTOL Unmanned Aerial Vehicle on a moving platform using optical flow," *Automatica*, 2010.

[11] B. Herisse, T. Hamel, R. Mahony, and F.-X. Russotto, "A nonlinear terrain following controller for a vtol unmanned aerial vehicule using translationnal optical flow," in *ICRA, Kobe, Japan*, 2009.

[12] H. K. Khalil, *Nonlinear Systems*. Prentice Hall, 2002.

[13] T. Hamel and R. Mahony, "Visual servoing of an under actuated dynamic rigid-body system: An image-based approach," *IEEE Transactions on robotics and automation*, vol. vol 18, pp. pp 187–198, April 2002.

[14] R. F. Vassallo, J. Santos-victor, and H. J. Schneebeli, "A general approach for egomotion estimation with omnidirectional images," *3rd Workshop on Omnidirectional Vision*, pp. 97–103, 2002.

[15] R. Mahony, P. Corke, and T. Hamel, "Dynamic image-based visual servo control using centroid and optic flow features," *Journal of Dynamic Systems, Measurement and Control*, vol. vol 130, pp. pp 011005–1–011005–12, January 2008.